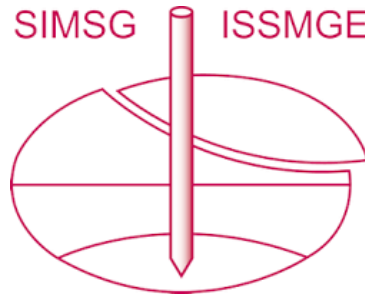


INTERNATIONAL SOCIETY FOR SOIL MECHANICS AND GEOTECHNICAL ENGINEERING



This paper was downloaded from the Online Library of the International Society for Soil Mechanics and Geotechnical Engineering (ISSMGE). The library is available here:

<https://www.issmge.org/publications/online-library>

This is an open-access database that archives thousands of papers published under the Auspices of the ISSMGE and maintained by the Innovation and Development Committee of ISSMGE.

The paper was published in the proceedings of the 10th European Conference on Numerical Methods in Geotechnical Engineering and was edited by Lidija Zdravkovic, Stavroula Kontoe, Aikaterini Tsiampousi and David Taborda. The conference was held from June 26th to June 28th 2023 at the Imperial College London, United Kingdom.

To see the complete list of papers in the proceedings visit the link below:

<https://issmge.org/files/NUMGE2023-Preface.pdf>

An insight into the thermodynamics-based elasto-plastic coupling of clays: role of voids and fabric anisotropy

F. Rollo¹, A. Amorosi¹

¹*Department of Structural and Geotechnical Engineering, Sapienza University of Rome, Roma, Italy*

ABSTRACT: This paper analyses the implications of two forms of isotropic and anisotropic thermodynamic-based elasto-plastic coupling on the constitutive response of clays. To this purpose, the single surface thermodynamic-based constitutive model for clays SANICLAY-T is adopted. Its hierarchical structure allows to introduce increasing complexity depending on the specific application, while the proper manipulation of potential functions leads to new forms of elasto-plastic coupling, driven by scalar and tensorial entities, characterised by a mutual influence between the elastic and plastic behaviour. The thermodynamic approach allows some relevant features of the phenomenon to be highlighted in more detail as compared to what conventionally derived from the elasto-plasticity theory, with particular reference to the effects of coupling on the yield domain in the Cauchy stress space and the resulting non-associated flow rule. Numerical simulations of laboratory tests illustrate the predictive capability of the model while ad hoc numerical simulations highlight the evolving and transient character of the anisotropic elasto-plastic coupling and its implications on the critical state.

Keywords: Thermodynamics; elasto-plastic coupling; anisotropy; clay

1 INTRODUCTION

In constitutive modelling of geomaterials it is common practice to use internal variables as descriptors of the state of the soil and its evolution due to any external perturbations. Within the framework of elasto-plasticity, a proper choice of the internal variables allows to describe macroscopically the soil behaviour that originates from the microscopic features such as particles arrangement, voids distribution, fissures and cracks and to keep track of their evolution. Moreover, the dependence of the reversible elastic response on the internal variables, whose evolution is eventually controlled by the plastic processes, introduces different forms of elasto-plastic coupling able to simulate the behaviour of soils when subjected to small perturbations, as discussed in Rollo & Amorosi (2022). The need for adopting the aforementioned internal variables instead of directly accounting for the plastic strains is dictated by the fact that they are measurable and do not depend on a reference configuration (e.g. Maugin, 2015).

In this perspective, the theoretical frame of reference called hyperplasticity (Houlsby & Puzrin 2006) allows to explore the implications of the elasto-plastic coupling on the soil response in a thermodynamic consistent way by the definition of two scalar functions: the free energy potential and the rate of dissipation. In this paper, two forms of elasto-plastic coupling of clays are presented based on the single surface plasticity model proposed by Rollo & Amorosi (2022): one is isotropic and controlled by the specific volume and the second one is anisotropic

and introduced through a second order fabric tensor that accounts for the orientation distribution of clay particles or aggregates. Both these internal variables can be evaluated based on appropriate experimental results: in fact the fabric tensor, which plays the role of the hardening parameter in the rotational hardening plasticity model, can either be evaluated by probing the material along different paths to detect the yield surface rotation or, under specific conditions, can be deduced by propagating shear waves along differently polarized planes, as discussed in Amorosi *et al.* (2021).

The thermodynamics-based elasto-plastic coupling brings remarkable consequences on the yield condition and on the associativeness of the flow rule, here analysed with reference to the results of a series of numerical simulations of ideal laboratory tests. Moreover, the results allow to draw some remarks on the role of the fabric anisotropy at critical state and on the use of elastic stiffness anisotropy as a proxy for soil fabric characterisation possibly supported by microstructural investigations.

2 FORMULATION OF THE MODEL

2.1 Internal variables

The specific volume represents a good scalar state variable to describe synthetically the average distribution and the changes of macropores size in clayey soils. In detail, specific volume and its rate are defined as:

$$v = \frac{V}{V_s} \quad ; \quad \dot{v} = \frac{\dot{V}}{V} - \frac{\dot{V}_s}{V_s} \quad (1)$$

where V is the total volume and V_s the volume of the solids. Recalling the definition of the total volumetric strain rate ($\dot{\varepsilon}_v = -\dot{V}/V$), assuming the additive decomposition of elastic and plastic strains ($\varepsilon = \varepsilon^e + \varepsilon^p$) and identifying the elastic volumetric strain rate with the variation of the solids volume according to Collins *et al.* (2010), one has:

$$\dot{\varepsilon}_v^e = -\frac{\dot{V}_s}{V_s} \quad ; \quad \dot{\varepsilon}_v^p = -\frac{\dot{v}}{v} \quad (2)$$

This assumption originally introduced for granular materials might also be plausible for clays, in which aggregates or cluster of particles can deform elastically, as discussed by Pedrotti & Tarantino (2018). Equation 2 implies that the specific volume can be adopted as suitable internal variable within the thermodynamic constitutive framework to describe the dissipative processes involved in permanent modifications of the voids distributions in clays. It is worth noting that, differently from Rollo & Amorosi (2022), here the specific volume is adopted in lieu of the preconsolidation pressure p_c , though they are related by:

$$\dot{p}_c = -\frac{p_c}{\lambda^*} \frac{\dot{v}}{v} \quad ; \quad p_c = p_r \left(\frac{v}{N} \right)^{-\frac{1}{\lambda^*}} \quad (3)$$

where N is the specific volume at the reference pressure p_r and λ^* a model parameter of the isotropic hardening law of the Cam clay-family plasticity models.

The other internal variable β is a second order fabric tensor accounting for the orientation distribution of its particles or aggregates, whose evolution is controlled by plastic strain rates as follows:

$$\dot{\beta} = c(\beta_b - \beta) \sqrt{\left(\dot{\varepsilon}_v^p + \beta : \dot{\varepsilon}^p \right)^2 + \frac{2}{3} (M^2 - \beta^2) \dot{\varepsilon}^p : \dot{\varepsilon}^p} \quad (4)$$

where M is the stress ratio at critical state and ε^p the deviatoric plastic strain tensor. β is the triaxial counterpart of β , $\beta = \sqrt{3/2 \beta : \beta}$, while c is a model parameter controlling the pace of the evolution and β_b represents the equilibrium ‘‘bounding’’ value, function of the current stress ratio $\mathbf{r} = \boldsymbol{\sigma}'/p$, with $\boldsymbol{\sigma}'$ deviatoric stress, for which the simplest expressions $\beta_b = \mathbf{r}/x$ (Dafalias & Taiebat, 2013) is adopted here, with x being a model parameter.

2.2 Thermodynamics-based formulation

A nonlinear anisotropic elastic formulation is adopted here, leading to the following Helmholtz free energy depending on the elastic strain as well as on the internal variables v and β :

$$\begin{aligned} \varphi(\boldsymbol{\varepsilon}^e, v, \beta) = & \left(\frac{v}{N} \right)^{\frac{r}{(n-1)\lambda^*}} \frac{P_r}{k(2-n)} k^{\frac{2-n}{1-n}} (1-n)^{\frac{2-n}{1-n}} \\ & \left\{ \left[k(1-n) - \frac{2}{3} g \right] \text{tr}^2(\boldsymbol{\varepsilon}^e - \omega \beta \beta \boldsymbol{\varepsilon}^e) + \right. \\ & \left. + 2g \text{tr} \left[\left(\boldsymbol{\varepsilon}^e - \omega \beta \beta \boldsymbol{\varepsilon}^e \right)^2 \right] \right\}^{\frac{2-n}{2-2n}} \end{aligned} \quad (5)$$

where n , k and g are elastic parameters and r and ω are additional model constants that control the dependency of the free energy on the internal variables. The derivative of Equation (5) with respect to the elastic strain leads to the Cauchy stress $\boldsymbol{\sigma}$ while differentiation with respect to the internal variables v and β leads to the generalised stresses $\bar{\chi}_v$ and $\bar{\chi}_\beta$, respectively, not reported here for the sake of brevity.

The other key ingredient of the model is the rate of dissipation, expressed as:

$$\begin{aligned} \dot{d}(\dot{\varepsilon}^p, \dot{\beta}, \dot{v}, v) = & \frac{P_r}{2} \left(\frac{v}{N} \right)^{\frac{1}{\lambda^*}} \left(\dot{\varepsilon}_v^p + \beta : \dot{\varepsilon}^p + \dot{d} \right) \\ & + \Lambda_1 \left(\frac{\dot{v}}{v} + \dot{\varepsilon}_v^p \right) + \Lambda_2 : \left[\dot{\beta} - c(\beta_b - \beta) \dot{d} \right] \end{aligned} \quad (6)$$

with

$$\dot{d} = \sqrt{\left(\dot{\varepsilon}_v^p + \beta : \dot{\varepsilon}^p \right)^2 + \frac{2}{3} (M^2 - \beta^2) \dot{\varepsilon}^p : \dot{\varepsilon}^p} \quad (7)$$

In Equation 7, Λ_1 and Λ_2 are Lagrangian multipliers that allow to introduce explicitly the rate of the internal variables \dot{v} and $\dot{\beta}$ within two terms that impose their evolutions by two constraints, thus not contributing to the amount of energy dissipated as they are numerically always equal to zero. The derivatives of Equation (6) with respect to the rates of plastic strains and internal variables lead to the dissipative generalised stresses χ , χ_v , χ_β and the singular Legendre transform provides the yield surface in the dissipative generalised stress space:

$$\begin{aligned}
 f(\boldsymbol{\chi}, \boldsymbol{\chi}_\beta, \chi_v, \boldsymbol{\beta}, v) = & \frac{3}{2}(\boldsymbol{\chi}' - \boldsymbol{\beta}\chi_p) : (\boldsymbol{\chi}' - \boldsymbol{\beta}\chi_p) + \\
 & + (M^2 - \beta^2)(\chi_p - v\chi_v)^2 + \\
 & - (M^2 - \beta^2)(\chi_p - v\chi_v) p_r \left(\frac{v}{N}\right)^{\frac{1}{\lambda^*}} + \\
 & + (M^2 - \beta^2) c\boldsymbol{\chi}_\beta : (\boldsymbol{\beta}_b - \boldsymbol{\beta}) p_r \left(\frac{v}{N}\right)^{\frac{1}{\lambda^*}} + \\
 & - (M^2 - \beta^2) [c\boldsymbol{\chi}_\beta : (\boldsymbol{\beta}_b - \boldsymbol{\beta})]^2 = 0
 \end{aligned} \quad (8)$$

By virtue of the Ziegler's principle it results $\boldsymbol{\chi} = \boldsymbol{\sigma}$, $\chi_v = \bar{\chi}_v$, $\boldsymbol{\chi}_\beta = \bar{\boldsymbol{\chi}}_\beta$ and the yield function in the Cauchy stress space can be obtained, though not reported here for the sake of conciseness. Further details can be found in Rollo & Amorosi (2022).

3 MODEL PERFORMANCE

The parameters r and ω control the isotropic and the anisotropic coupling on the internal variables v and $\boldsymbol{\beta}$, respectively and when both are zero the SANICLAY-T model (Rollo & Amorosi, 2020) is recovered.

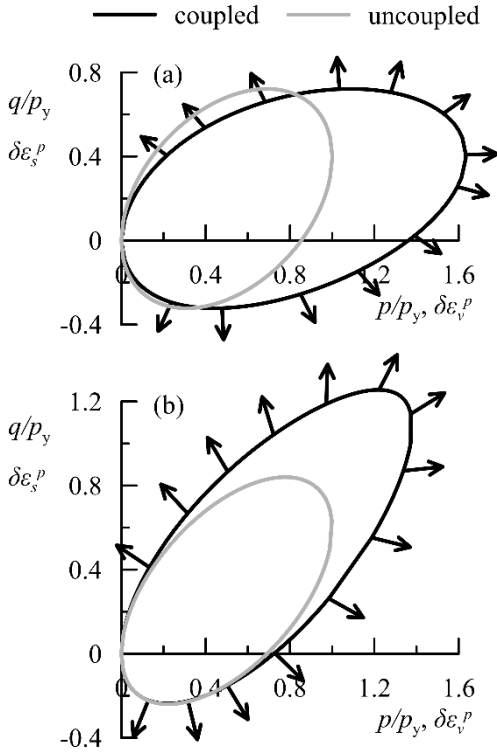


Figure 1. Yield surfaces with $\beta = 0.4$ and (a) $\omega = 0$ and (b) $r = 0$. The arrows denote the plastic strain rates

The elasto-plastic coupling modifies the shape of the yield surface in the stress space and produces a non-associated flow rule. Figure 1 shows the triaxial representation of the yield surface of the model for the (a) isotropic and (b) anisotropic coupling in the normalised $p/p_y - q/p_y$ plane, with p_y the maximum (i.e. preconsolidation) pressure and p and q the mean effective pressure and deviatoric stress, respectively, with the model parameters of Table 1. The black arrows in Figure 1 indicate the direction of the plastic strain rates.

To explore the effects of the elasto-plastic coupling on the response of the model as compared to the uncoupled formulation, a series of numerical simulations at the material point level are shown. For simplicity, while highlighting the role of the isotropic coupling, the model is scaled to the Modified Cam clay (i.e. $\boldsymbol{\beta} = \mathbf{0}$, $\dot{\boldsymbol{\beta}} = \mathbf{0}$). Figure 2 shows the results of ideal simulations of isotropically consolidated undrained triaxial tests for different initial values of mean effective pressure and $v = 1.513$ adopting the model parameters of Table 1.

Table 1. Model parameters

Parameter	Value	Parameter	Value
p_r (kPa)	100	M	1.0
n	0.8	λ^*	0.07
k	67	c	100
g	50	x	2.0
r	0.4 (0)	ω	0 (1.0)
N	1.8		

Figure 2 shows the stress paths and the stress-strain response for the coupled formulation ($r = 0.4$) and the uncoupled one ($r = 0$), together with the initial yield surfaces. The elastic response is characterised by a volumetric-deviatoric coupling as a consequence of the non-linear hyperelastic formulation that produces the curvature of the stress paths and an increase of the elastic stiffness with the current stress/strain. The dependence of the free energy on the specific volume, accounted for when $r = 0.4$, increases the elastic stiffness, as observed from the stress-strain curves. Moreover, the different shape and size of the initial yield surface and the non-associated flow rule that stem from the elasto-plastic coupling govern the response when plasticity is engaged. These features not only produce a deviation of the stress paths and the stress-strain curves from those obtained for the uncoupled formulation, but also modify the stress ratio at critical state (i.e. lower than M): these aspects should be taken into account in the calibration of the model parameters on results of laboratory tests on natural and reconstituted clays.

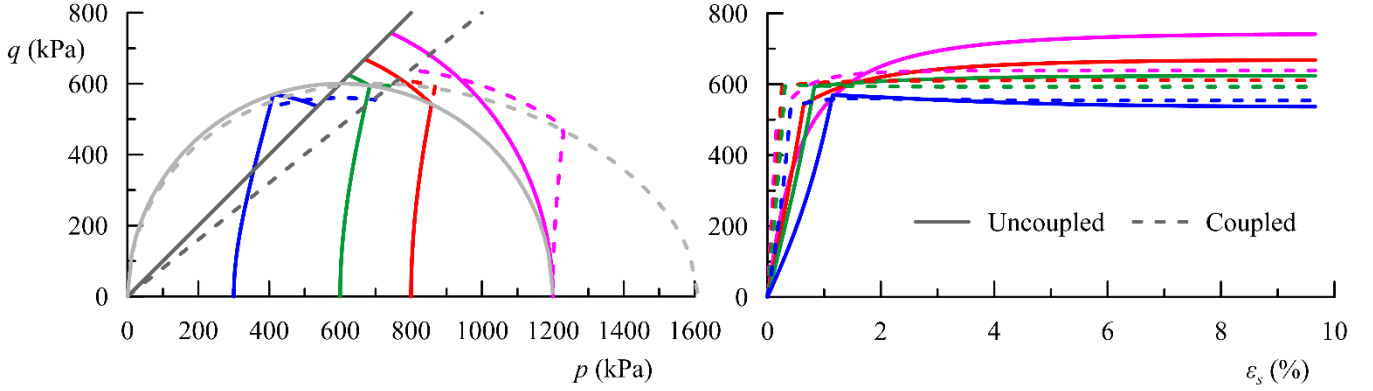


Figure 2. Simulations of isotropically consolidated undrained triaxial tests for different initial stresses for the coupled ($r = 0.4$) and uncoupled ($r = 0$) MCC model.

Similar conclusions can be drawn with reference to the results of simulations of isotropically consolidated drained triaxial tests shown in Figure 3 in terms of stress-strain curves and volumetric strains ε_v .

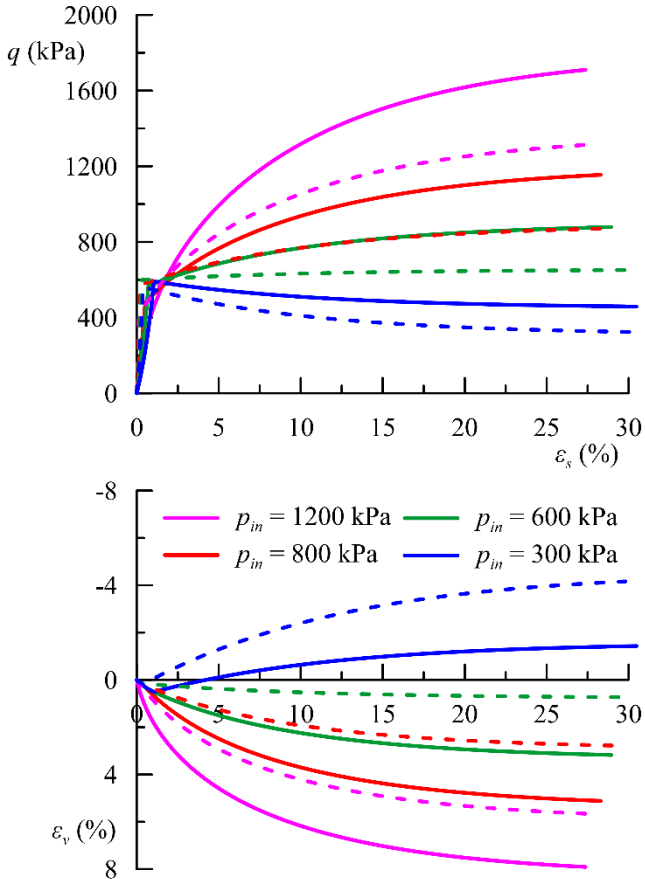


Figure 3. Simulations of isotropically consolidated drained triaxial tests for the MCC model and different initial stresses. The continuous and dashed lines denote the uncoupled and coupled formulations, respectively.

Analogously to the isotropic coupling, in what follows the main features of the anisotropic elasto-plastic coupling are illustrated with reference to numerical simulations of ideal experimental conditions. For this purpose, the isotropic coupling is not considered ($r = 0$)

while the coupling via the rotational hardening internal variable is taken into account ($\omega = 1$) and its effects are compared to the results of the uncoupled model ($\omega = 0$). Calculations are performed considering an initial specific volume $v = 1.777$ and with the model parameters reported in Table 1. Figure 4 shows the results of numerical simulations of isotropically consolidated undrained triaxial test for a normal consolidated clay. The initial yield surface coincides with the Modified Cam clay ellipse as the material is initially isotropic ($\beta = \mathbf{0}$) and assumes the final distorted shape shown in Figure 4(a) when the critical state condition is reached. It is clear that the coupling plays a role when $\beta \neq \mathbf{0}$ and as long as β differs from its equilibrium value: the greater is the difference $\|\beta_b - \beta\|$, the more relevant is the contribution of the elasto-plastic coupling to the results. Not surprisingly, the anisotropic formulation exhibits transient elasto-plastic coupling effects, as they only hold while the related tensorial internal variable evolves, whereas isotropic elasto-plastic effects are permanent, as driven by the actual value of the corresponding scalar internal variable v . The yield surfaces and the flow rules obtained with the coupled and uncoupled formulations coincide at the initial and final states as at critical state the equilibrium bounding value β_b is attained. Nevertheless, the responses of the coupled and uncoupled formulations in terms of stress paths and deviatoric strains keep track of the loading history experienced by the material. It is worth mentioning that the evolving character of the rotational hardening internal variable is also directly related to the evolving elastic anisotropy, as shown in Figure 4(c) in terms of anisotropy ratio G_{hh}/G_{hv} between the elastic shear moduli ratio G_{hh} and G_{hv} , evaluated by double differentiation of Equation 5 with respect to ε^e , where subscripts h and v stand for horizontal and vertical, respectively. The evolving character can be obtained only if the elasto-plastic coupling is considered in the formulation; otherwise, the fabric tensor would obviously be constant and, in the specific simulation, the material would remain isotropic.

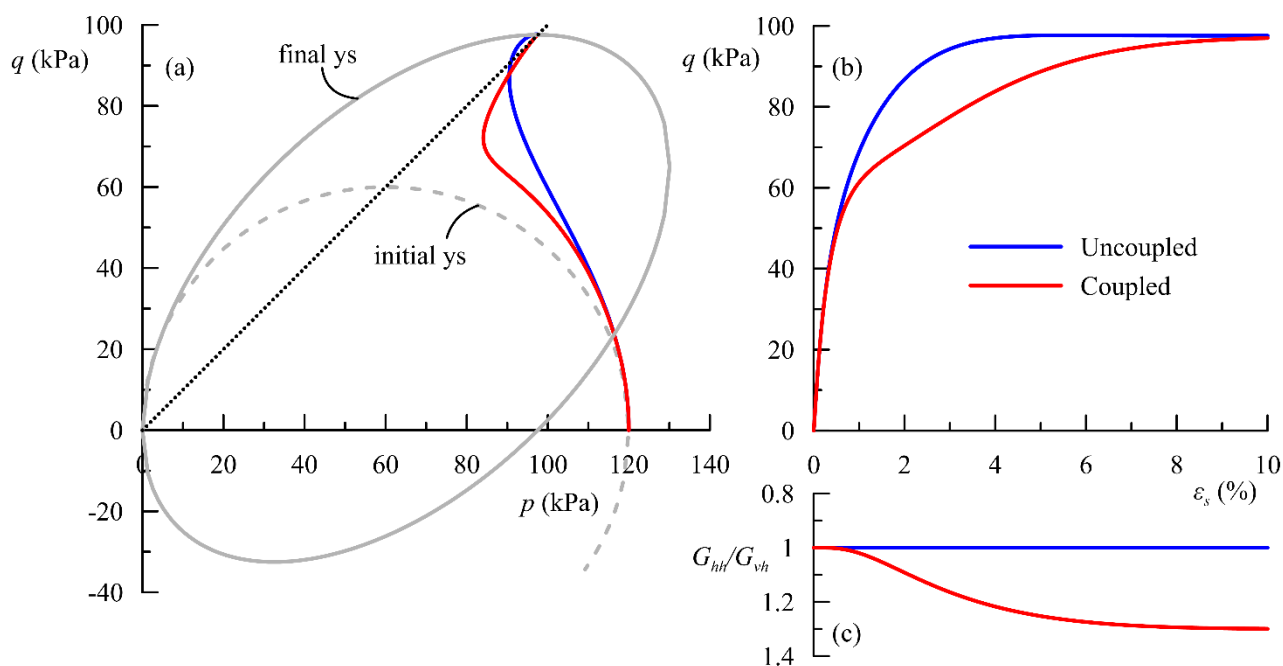


Figure 4. Simulations of isotropically consolidated undrained triaxial tests for normal consolidated clay for the coupled ($\omega = 1.0$) and uncoupled ($\omega = 0$) formulations

Finally, ideal drained simple shear tests are performed to highlight the tensorial character of the anisotropic coupling and to figure out the model response along a stress path that induces a rotation of the principal directions of the stress and fabric tensors. The initial specific volume is 1.777 and the stress state is initialised under K_0 conditions ($K_0 = 0.6$) at $p = 66$ kPa (OCR = 2), while the rotational hardening β is initialised consistently with the stress through $\beta = \mathbf{r}/x$, leading to $\beta = \eta_{K_0}/x = 0.2$. Subsequently, shear strain (γ) controlled simulations are carried out leading to the raise of shear stress τ as shown in Figure 5. Since the test is performed under plane strain conditions, the out-of-plane direction is always a principal one, while a rotation of the principal directions of σ and β occurs in the shearing plane and can be quantified through the angle α with respect to the horizontal direction as sketched in Figure 5. The principal values (i.e. eigenvalues) of β are also computed. As the shear stress τ increases, the horizontal stress components σ_h acting on the constrained (i.e. vertical) planes evolve until they equate the vertical one σ_v at critical state. This process involves a rotation of the principal directions of σ from the initial triaxial configuration ($\alpha = 0^\circ$) until the final value $\alpha = 45^\circ$. A similar, though delayed trend governed by the plastic process is observed for β : the principal directions of the fabric tensor coincide with the horizontal and vertical ones as long as the response is elastic but when the yield surface is reached they start rotating towards the value of 45° . Not surprisingly, when β reaches the bounding

value the stress and fabric tensor become coaxial as β_b is proportional to the deviatoric stress. Therefore, at the end of the process only the shear-like component of β related to the shear stress is non-zero and, consistently, the maximum and minimum eigenvalues have the same magnitude but opposite sign.

Figure 5 reveals that the elasto-plastic coupling modifies the stress-strain response of the model as compared to the uncoupled formulation only in the transitional regime and marginally affects the evolution of the principal values and directions of stress and fabric. However, the elasto-plastic coupling keeps track of the evolution of the elastic stiffness anisotropy during the loading process. In simple shear test the ratio G_{hh}/G_{vv} depends on the elasto-plastic coupling as well as on the current stress by virtue of the nonlinear hyperelasticity. Therefore, the results obtained for $n = 0$ (linear elasticity) are also shown to isolate the contribution of the elasto-plastic coupling. Comparison between Figure 4c and Figure 5 indicates that different values of G_{hh}/G_{vv} are reached at critical state depending to the loading path. In fact, the model requires the invariance of β (i.e. the norm of the fabric tensor β) at critical state, that does not exclude the possibility of having different components of the fabric tensor, and hence different asymptotic anisotropy ratios according to the stress path. Naturally, at this point one question arises: should the critical state be anisotropic and if so, should the stiffness anisotropy be dependent on the followed stress path and the final stress configuration? There is no definitive answer to this question, which is still a debated issue among the geotechnical community. However, for granular materials

the idea of an anisotropic critical state (Dafalias, 2016) is getting gradually more attractive as supported by preliminary experimental observations (Zhao *et al.*, 2021) and discrete element analyses (Wang *et al.*, 2020). For clays the trend is less clear but microstructural investigations that combine scanning electron microscopy and X-ray microtomography (Gao *et al.*, 2020) suggest that the clusters of particles tend to assume a more iso-oriented arrangement according to the applied state of stress when approaching the critical state. However, despite the open challenge of experimentally exploring the behaviour of the clay in this configuration, the identification of an anisotropic form of elastic-plastic coupling may justify the use of reversible regime data as a proxy for detecting the fabric anisotropy at critical state.

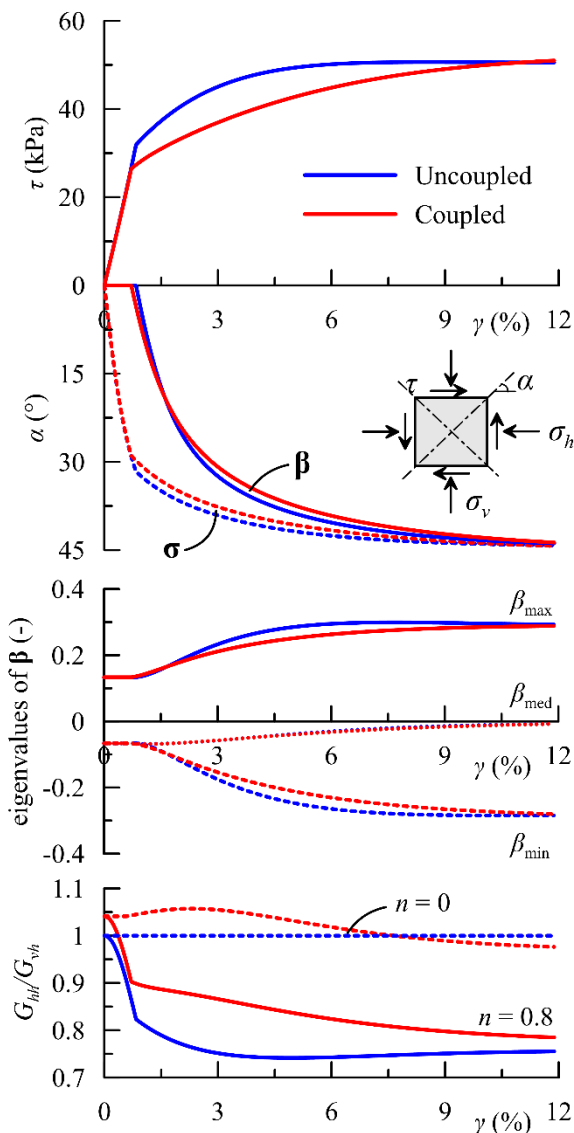


Figure 5. Simulations of anisotropically consolidated (K_0 -conditions, $\beta = 0.2$) drained simple shear tests

4 CONCLUSIONS

This paper presents the results of a new constitutive model for clayey soils characterised by two forms of elasto-plastic coupling developed within the framework

of hyperplasticity. The first one is isotropic and is introduced by a dependence of the elastic free energy on the specific volume, while the second one is controlled by the rotational hardening law and takes into account the evolving character of the small strain stiffness anisotropy when irreversible plastic strains occur. Numerical simulations show the effects of elasto-plastic coupling based on the stress-strain response and shed new light on the role of fabric anisotropy at critical state.

5 ACKNOWLEDGEMENTS

The authors acknowledge the support by the research project RETURN - multi-Risk sciEence for resilientT commUnities undeR a changiNg climate - funded by the European Union within the Italian Recovery and Resilience Plan (PNRR).

6 REFERENCES

- Amorosi, A., Rollo, F., & Dafalias, Y. F. 2021. Relating elastic and plastic fabric anisotropy of clays. *Géotechnique*, **71**(7), 583-593. <https://doi.org/10.1680/jgeot.19.P.134>.
- Collins, I. F., Muhunthan, B., & Qu, B. 2010. Thermomechanical state parameter models for sands. *Géotechnique*, **60**(8), 611-622.
- Dafalias, Y. F., & Taiebat, M. 2013. Anatomy of rotational hardening in clay plasticity. *Géotechnique*, **63**(16), 1406-1418.
- Dafalias, Y. F. 2016. Must critical state theory be revisited to include fabric effects?. *Acta Geotechnica*, **11**, 479-491.
- Gao, Q. F., Hattab, M., Jrad, M., Fleureau, J. M., & Hicher, P. Y. 2020. Microstructural organization of remoulded clays in relation with dilatancy/contractancy phenomena. *Acta Geotechnica*, **15**, 223-243.
- Houlsby, G. T., & Puzrin, A. M. 2006. *Principles of hyperplasticity*. Springer - Verlag London Limited.
- Maugin, G. A. 2015. The saga of internal variables of state in continuum thermo-mechanics (1893–2013). *Mechanics Research Communications*, **69**, 79-86.
- Pedrotti, M., & Tarantino, A. 2018. An experimental investigation into the micromechanics of non-active clays. *Géotechnique*, **68**(8), 666-683.
- Rollo, F., & Amorosi, A. 2022. Isotropic and anisotropic elasto-plastic coupling in clays: a thermodynamic approach. *Int. Journal of Solids and Structures*, **248**, 111668. <https://doi.org/10.1016/j.ijsolstr.2022.111668>
- Rollo F., Amorosi A. 2020. SANICLAY-T: Simple thermodynamic-based anisotropic plasticity model for clays. *Computers and Geotechnics*, **127**, 103770. <https://doi.org/10.1016/j.comgeo.2020.103770>.
- Wang, R., Dafalias, Y. F., Fu, P., & Zhang, J. M. 2020. Fabric evolution and dilatancy within anisotropic critical state theory guided and validated by DEM. *Int. J. of Solids and Structures*, **188**, 210-222.
- Zhao, C. F., Pinzón, G., Wiebicke, M., Andò, E., Kruyt, N. P., & Viggiani, G. 2021. Evolution of fabric anisotropy of granular soils: X-ray tomography measurements and theoretical modelling. *Computers and Geotechnics*, **133**, 104046.